IOPscience iopscience.iop.org

Home Search Collections Journals About Contact us My IOPscience

Model of the H-mode in tokamaks

This content has been downloaded from IOPscience. Please scroll down to see the full text.

1989 Nucl. Fusion 29 1031

(http://iopscience.iop.org/0029-5515/29/6/013)

View the table of contents for this issue, or go to the journal homepage for more

Download details:

IP Address: 142.132.1.147
This content was downloaded on 28/08/2014 at 06:14

Please note that terms and conditions apply.

MODEL OF THE H-MODE IN TOKAMAKS

S.-I. ITOH*
Institute for Fusion Theory,
Hiroshima University,
Hiroshima

K. ITOH*
Plasma Physics Laboratory,
Kyoto University
Kyoto

Japan

ABSTRACT. The paper presents a theoretical model of the H-mode in tokamaks which is based on the bifurcation of the radial electric field at the plasma edge. The electric field is determined by the balance of the non-ambipolar fluxes of ions and electrons at the edge. It is found that bifurcations of the radial electric field, the particle flux and the convective energy loss occur when the edge gradient reaches a critical value. This is attributed to L-H or H-L transition. The critical conditions are examined and the role of neutral particles as well as the effect of impurities are incorporated in the model. Combining the confinement scaling laws for both the core plasma and the scrape-off layer plasma, the threshold power for the transition is derived. The temporal evolution associated with the transition is studied.

1. INTRODUCTION

The H-mode, which was first observed in ASDEX [1], was also found in many other tokamaks with various heating methods [2–8]. The database for the transition condition, the improvement of global confinement and the transport properties in the core plasma was extended [9–12]. The H-mode phenomena constitute a new aspect in investigations of anomalous plasma transport. Understanding of the H-mode is also required for a prediction of the confinement in next generation tokamaks. Control of the H-mode is likely to be necessary for ignition to become possible.

The H-mode involves phenomena in various regions of the tokamak plasma, such as a change in stored energy in the core plasma, formation of a pedestal at the edge, a density decrease in the scrape-off layer (SOL) and a change in the properties of the divertor plasma. Although theoretical work on H-mode modelling has been performed [13–23], the physics of the H-mode has not yet been fully explained. The most important factor in modelling is the causality of H-mode related phenomena. Recently, it has been shown experimentally that the H-mode transition occurs at the plasma edge (inside of the outermost magnetic surface). The improvement of confinement then propagates into the core region. As a result of the reduced loss of the main plasma, the density of the SOL plasma decreases. One of the key problems in the investigation of the H-mode is the transition phenomena at the plasma edge.

The characteristics of the H-mode transition are: (1) the heat flux carried by the charged particles across the plasma surface decreases very rapidly [24], (2) pedestal formation begins at the edge and proceeds inwards [25], and (3) a pedestal is established after the transition [25, 26]. The transition occurs in both separatrix and limiter configurations [27, 28]. Experimental observations suggest that the transition originates from a change of the transport inside the outermost magnetic surface.

The parameter space regime in which the transition can occur has been studied experimentally. The condition necessary for transition has been discussed either in terms of global parameters, such as heating power and density [26, 28–30], or in terms of local parameters, such as the collisionality at the edge [31–33]. Since the occurrence of transition is delayed after the onset of heating [34] and since the H-mode is observed even in an Ohmic plasma [26], it is concluded that there must be a critical condition (local values of density and temperature and/or their gradients) for induction of transition. A certain amount of power is necessary to realize the critical edge condition.

* Present address: National Institute for Fusion Science, Nagoya, Japan.

The change of the transport properties of the core plasma during the H-phase has also been studied and a reduction of the thermal diffusivity has been found [25]. The improvement of energy confinement in the core plasma is usually accompanied by a density increment in the H-phase compared to the L-phase, so that it has not been possible to determine the actual cause of the improvement.

To find an explanation for these experimental observations, we study the mechanism of the L- to H-mode transition (or that of the H- to L-mode transition). We concentrate on the transition phenomena. We do not analyse the changes in the core plasma or those in the SOL, which are induced as a result of the transition at the edge.

Under conditions close to those for which transition occurs, the transport coefficient seems to have two or more values for a given plasma profile. This ansatz can be accepted if the pedestal formation, i.e. the rapid change in plasma parameters, begins after the reduction of the energy loss. The loss can assume two different values for one profile at the onset of the transition. Bifurcation of the electric field could be one of the hidden variables to explain the multiple values of the flux.

In this article, we study the possible mechanism of the L- to H-mode (H- to L-mode) transition associated with changes in particle and convective energy losses near the plasma edge. The non-ambipolar loss of ions near the edge has been discussed first by Hinton and Ohkawa [15, 19]. Extending their theory, we include the non-ambipolar electron loss in our study to obtain a consistent radial electric field. Bifurcations of the electric field and the convective losses have been predicted for the case where the edge gradient reaches a threshold value [21]. We have refined the simple model of Ref. [21] for the case where the plasma is subject to toroidal rotation. In this refined model, the flux can take multiple values for the same density/temperature conditions at the plasma edge. This applies for both limiter and separatrix configurations. We analyse the dependence of the critical condition on the geometry, such as the location of the limiter, and study the temporal evolution associated with the transition. We combine the critical condition with a transport model of the edge plasma in the L-phase and obtain a scaling law of the threshold power for the L- to H-mode transition. A reduction of the fluctuation after the transition is observed.

In the following, we use the notation H/L transition when we refer to both the L- to H-mode and the H- to L-mode transitions. In cases where the direction of the transition is important, we write L- to H-mode transition and H- to L-mode transition.

2. MODEL OF PARTICLE FLUXES

We consider the surface of a circular tokamak plasma defined by the limiter which is located at the poloidal angle $\theta = \theta_m$, as shown in Fig. 1. Toroidal co-ordinates (r, θ, φ) are introduced and axial symmetry, $\partial/\partial\varphi = 0$, is employed. We take the low beta ordering and assume that

$$B_\phi = \frac{B_t}{1 + (r/R)\cos\theta} \tag{1}$$

$$B_\theta = B_p\left[1 + \Lambda\frac{r}{R}\cos\theta\right] \tag{2}$$

where R is the major radius. These assumptions are not essential in the following argument. In this configuration, we study the losses of ions and electrons near the edge. For the divertor configuration, the poloidal angle of the X-point corresponds to θ_m.

The particle loss of the j-th species (j = i,e) is written as

$$\Gamma_j = \Gamma_j^A + \Gamma_j^{NA} \tag{3}$$

where the superscripts A and NA stand for the ambipolar and non-ambipolar parts, respectively. The heat flux is expressed as

$$q_j = q_{cond,j} + T_j\Gamma_j \tag{4}$$

where q_{cond} is the conductive energy flux and T is the temperature. The electric field is determined by the balance of the non-ambipolar parts of particle fluxes.

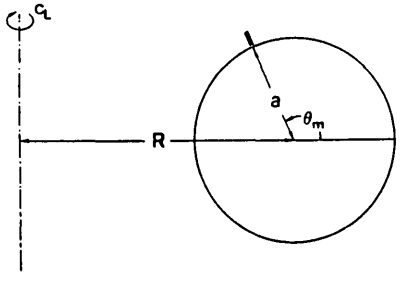

FIG. 1. Schematic geometry of the analysis. $\theta = 0$ is taken at the outside of the torus. The location of the limiter (x-point for the separatrix) is defined by the poloidal angle θ_m.

There is a bifurcation of the electric field [21], which is determined by the ambipolarity equation

$$\sum_k Z_k \Gamma_k^{NA}(E_r) = \Gamma_e^{NA}(E_r) \tag{5}$$

where Z_k is the ionic charge number and the summation is taken for ions. The change of the electric field affects the intrinsic non-ambipolar fluxes. The ambipolar part of the particle flux and the convective part of the heat flux also depend on the radial electric field. The bifurcation of the electric field can also affect the conductive loss.

2.1. Non-ambipolar ion loss

We first study the ion loss which does not satisfy the intrinsic ambipolarity. Of the various non-ambipolar ion losses, we study the loss by the loss cone and the loss by charge exchange in the collisionless regime. We do not take into account the non-ambipolar anomalous ion loss. The trapped ions, which have a large banana width ρ_b, can escape from the confined region by interacting with the material limiter or by moving to the divertor region across the separatrix. For the electrons, this loss is negligible because of the small poloidal gyroradius.

The direct loss of ions is important when we study the region $|a-r| \lesssim \rho_p$, where a is the plasma minor radius, $\rho_p = v_{Ti} mqR/aB_t$ is the poloidal gyroradius, q is the safety factor and v_{Ti} is the thermal velocity of ions. In this region, the ion loss is given by (see Ref. [15])

$$\Gamma_i = n_i \nu_i \rho_p \frac{1}{\sqrt{\epsilon}} \hat{F} \tag{6}$$

where n_i is the ion density, ϵ is the inverse aspect ratio r/R, ν_i is the ion–ion collision frequency and $\hat{F}$ is proportional to the relative number of ions in the loss cone in velocity space, with $0 < \hat{F} < 1$. We neglect the weak dependence of the loss on the mirror ratio. The loss flux is proportional to the thickness Δ of the region in which the loss through the loss cone is important, and we choose $\Delta = \rho_p$. The flux Γ_i^{NA} is evaluated by averaging over this region. The effect of non-uniformity is discussed in Section 5.

In the presence of a radial electric field the coefficient $\hat{F}$ is the key factor in determining the bifurcation. As the radial electric field builds up, the ions start to rotate [35, 36]. The poloidal rotation of transit particles is damped owing to ion collisions [36–38] and the rotation changes to *toroidal* rotation in the stationary state. The trapped particles, which play a main role in non-ambipolar loss, rotate in the toroidal direction. In a previous article [21], we have estimated the loss reduction on the basis of the poloidal rotation due to the E × B drift. In the present paper we study the effect of toroidal rotation on E_r. We find that the qualitative nature of the function $\hat{F}$ does not depend on the assumptions made in Ref. [21].

The reduction of the ion loss originates from the shift of the loss cone away from the peak of the distribution function f_i in velocity space. At the appearance of the electric field, the ion distribution function relaxes to a new form. If the ions rotate in the toroidal direction, the distribution function is shifted in velocity space. The form of f_i is given by a Maxwellian in the rotating frame [38] as

$$f_i \propto \exp\left[-\frac{(v_\parallel - R\omega_E)^2}{v_{Ti}^2}\right] \tag{7}$$

where ω_E is the toroidal rotation frequency

$$\omega_E = \frac{E_r}{RB_p} \tag{8}$$

Up to the order of ϵ^0, the shift of the loss cone is the same as that of the distribution function in velocity space [39].

For calculation of the change of the loss in the toroidal rotation limit, we obtain the higher order correction with respect to ϵ. The ion orbit in the presence of the radial electric field is discussed in the Appendix. If we take into account corrections up to the order of $\sqrt{\epsilon}$, the relative shift of the loss cone in velocity space is

$$v_c = \sqrt{2\epsilon(1 - \cos\theta_m)}\, R\omega_E \tag{9}$$

as is shown in Fig. A-1. The notation v_c indicates the lower limit of the parallel velocity in the rotating frame for ions to interact with the limiter and to be lost. In this frame, the minimum energy of ions appearing in the loss cone is $mv_c^2/2$. The minimum energy of the loss cone depends also on the distance of the magnetic surface from the plasma surface, i.e. $a - r$ (v_c has a radial dependence). We use here the averaged flux. Using Eq. (9), we can estimate the ratio of the loss particles and the expression for Γ_i is

$$\Gamma_i = \frac{F}{\sqrt{\epsilon}} n_i \nu_i \rho_p \exp\left\{-\sigma\left(\frac{\rho_p e E_r}{T_i}\right)^2\right\} \tag{10}$$

$$\sigma = 2\epsilon(1 - \cos\theta_m) \tag{11}$$

where F is a numerical coefficient of order unity.

Comparing Eqs (10) and (11) with Eq. (2) of Ref. [21], we find a difference in the coefficient of the exponent. The dependence of Γ_i on E_r is the same. The coefficient $\sigma = 2\epsilon(1 - \cos\theta_m)$ indicates the importance of the location of the ion sink (limiter/X-point). For the case where the sink is located at the outside of the torus, the reduction of the ion loss is small. When θ_m is of the order of $\pi/2$, the coefficient is close to unity. In the actual experiment, the difference between the poloidal rotation limit and the toroidal rotation limit is small. If θ_m is $O(\sqrt{\epsilon})$, we have to calculate the higher order correction of ϵ.

We now evaluate the ion loss due to charge exchange. With toroidal rotation, the charge exchange with neutral particles reduces the ion momentum without transferring it to electrons. The importance of this mechanism in the L/H transition has been pointed out in Ref. [23]. This momentum imbalance causes a non-ambipolar loss of ions. The toroidal velocity is given as (see Refs [35, 36])

$$v_\phi = -\frac{qT_iR}{erB}\left\{\frac{1}{n_i}\frac{dn_i}{dr} + \frac{C_i}{T_i}\frac{dT_i}{dr} - \frac{e}{T_i}E_r\right\} \tag{12}$$

where C_i is a numerical coefficient close to unity. The rate of the charge exchange is given as $n_0\langle\sigma_{cx}v\rangle$, where n_0 is the density of the neutral particles, σ_{cx} is the charge exchange cross-section and $\langle\ \rangle$ indicates the average over the ion distribution. The loss of ions due to the charge exchange is given as (see Refs [23, 36])

$$\Gamma_{i,cx} = \frac{qR}{erB}\frac{\Delta_n}{\rho_p} n_0\langle\sigma_{cx}v\rangle m_i n_i v_\phi \tag{13}$$

where Δ_n denotes the penetration length of neutral particles near the plasma boundary. The charge exchange loss consists of trapped particles and transit particles. Summing up Eqs (10) and (13), the non-ambipolar ion loss is given as

$$\Gamma_i^{NA} = \left[\nu_i \frac{F}{\sqrt{\epsilon}}\rho_p \exp(-\sigma X^2) + \Delta_n n_0\langle\sigma_{cx}v\rangle(\lambda_i + X)\right] n_i \tag{14}$$

where

$$\lambda_i = -\rho_p\left\{\frac{1}{n_i}\frac{dn_i}{dr} + \frac{C_i}{T_i}\frac{dT_i}{dr}\right\} \tag{15a}$$

$$X = \frac{\rho_p e E_r}{T_i} \tag{15b}$$

2.2. Non-ambipolar electron loss

We study now the non-ambipolar electron loss. The electron transport is dominated by anomalous processes. The origin of the anomalous loss near the plasma surface has not yet been identified. Theories suggest that microscopic instabilities may generate an anomalous electron flux [40]. The anomalous electron flux may be explained by $E \times B$ motion associated with the instability. As discussed in Refs [41–43], the ambipolarity of this anomalous flux originates from the local momentum balance between electrons and ions via the excited waves. In a sheared magnetic configuration, the waves having a frequency in the range of the drift wave frequency propagate a distance δ_w across the magnetic surfaces. At this distance, $k_\parallel v_{Ti} \sim \omega$ holds and the wave is absorbed by ions. If the wave is excited in the region $|a - r| < \delta_w$, the wave takes away the momentum to the SOL plasma before being absorbed by ions. This mechanism causes the non-ambipolarity of the anomalous electron flux. Evaluating $\omega \sim \omega_* \sim \kappa c_s k\rho_i$ ($\kappa = -\nabla n/n$), δ_w is estimated as $\delta_w/\rho_p \sim (q\kappa/q')$. The relation

$$\Delta \lesssim \delta_w \tag{16}$$

is usually satisfied. We therefore conclude that the electron loss in the region of interest can be non-ambipolar.

The anomalous electron flux depends on the radial electric field. Part of this dependence comes from the mobility, and we can write, according to Refs [41, 42],

$$\Gamma_e^{NA} = -D_e n_e\left\{\frac{1}{n_e}\frac{dn_e}{dr} + \frac{\alpha}{T_e}\frac{dT_e}{dr} + \frac{e}{T_e}E_r\right\} \tag{17}$$

where α is a numerical constant of the order of unity. D_e can be expressed in terms of the local turbulence spectrum. In principle, D_e may depend on the radial electric field and on θ_m. The radial electric field affects the stability of the microscopic modes. We neglect here the E_r and θ_m dependences of D_e.

3. BISTABLE SOLUTION

The solution of the ambipolar equation is valid for the stationary state. Using Eqs (14) and (17), we study the bistable solution near the plasma edge.

3.1. Ambipolar condition

Equating the electron flux and the ion flux, we have the equation which determines the electric field in the stationary state. Substituting Eqs (14) and (17) into Eq. (5), we have

$$\exp(-\sigma X^2) + d_n(X + \lambda_i) = d(\lambda - X) \tag{18}$$

where

$$d_n = \frac{\sqrt{\epsilon}\, n_0 \langle \sigma_{cx} v \rangle}{\nu_i F} \frac{\Delta_n}{\rho_p} \tag{19a}$$

$$d = \frac{\sqrt{\epsilon}\, D_e}{\nu_i F \rho_p^2} \tag{19b}$$

$$\lambda = -\frac{T_e}{T_i} \rho_p \left\{ \frac{1}{n_e} \frac{dn_e}{dr} + \frac{\alpha}{T_e} \frac{dT_e}{dr} \right\} \tag{19c}$$

In Eq. (18), the first term on the left hand side is the contribution of the ion loss due to the loss cone, the second term comes from the charge exchange loss of ions in the presence of toroidal rotation, and the right hand side is the flux of electrons. The normalized flux $\hat{\Gamma}$ is introduced as

$$\hat{\Gamma} = \Gamma^{NA} \frac{\sqrt{\epsilon}}{n_i \nu_i \rho_p F} \tag{20}$$

The convective energy loss associated with the non-ambipolar flux is given as $q_{conv}^{NA} = (T_e + T_i)\Gamma^{NA}$.

3.2. Bifurcation and critical condition

Equation (18) predicts the transition from a singular solution to a bifurcated solution at particular values of the parameters. Figure 2 illustrates the normalized flux $\hat{\Gamma}_{e,i}$ in the absence of neutral particles, $d_n = 0$, as a function of $\rho_p eE_r/T_i$. The dependence of D_e on E_r is neglected here. In this limiting case, Eq. (18) is rewritten as

$$\exp(-\sigma X^2) = d(X - \lambda) \tag{21}$$

As seen from Fig. 2, the transition is also predicted by the simplified Eq. (21). When the gradient is weak and λ is small, Eq. (21) has one real solution. With an increase in λ or d, a bifurcation of the solution sets in (dashed lines in Fig. 2). For a fixed value of d, the transition occurs at the critical value λ_c. The solution indicated by A is characterized by a large flux (branch L) and the solution indicated by D has a smaller flux (branch H). The criterion of the transition is given by the solution C.

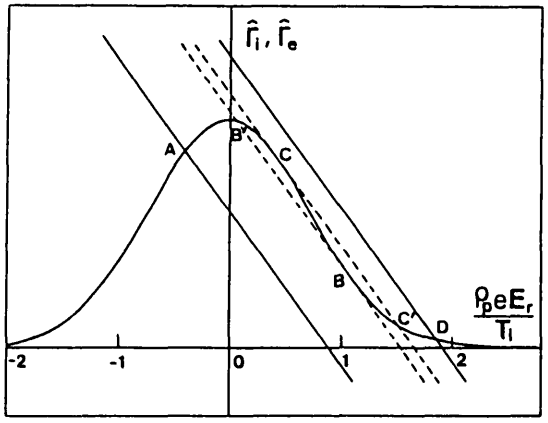

FIG. 2. Non-ambipolar fluxes of ions (denoted by i) and electrons (denoted by e) as a function of the radial electric field. Normalized values are shown. At particular values of λ (denoted by dashed lines), transitions occur.

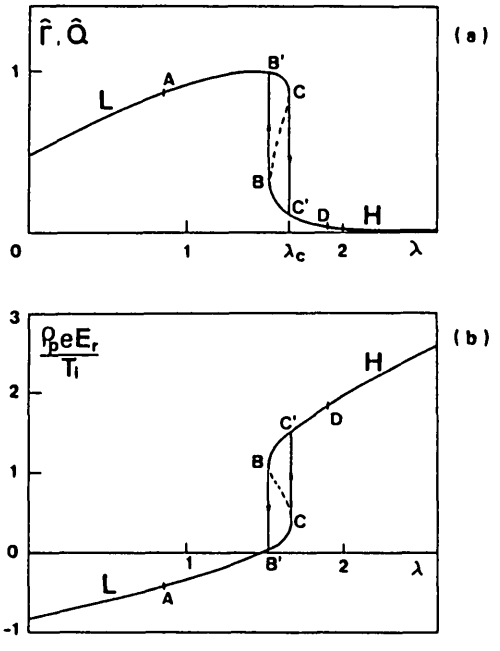

FIG. 3. (a) Normalized particle and convective heat fluxes as a function of the edge gradient λ. (b) Associated change of the radial electric field. There are no neutral particles, $d_n = 0$.

Figure 3 illustrates the λ dependence of the normalized flux $\hat{\Gamma}$ in the absence of neutral particles. The associated change of the radial electric field is shown in Fig. 3(b). A cusp-type catastrophe [44, 45] (Riemann-Hugoniot catastrophe) appears. The solutions of Eq. (21) form a cusp-type surface in the space (λ, d, E_r (or $\hat{\Gamma}$)). When λ is below λ_c, the electric field is negative (directed inward) or weakly positive and the fluxes are large. When λ exceeds λ_c, the electric field becomes positive and the fluxes are reduced. After the transition C → C′, the particle flux Γ^{NA} and the convective energy flux q_{conv}^{NA} decrease by more than a factor of ten. In the branch of the lower fluxes, the electric field has the approximate value

$$E_r = \frac{\lambda T_i}{e\rho_p} \quad (\lambda \gtrsim \lambda_c) \tag{22}$$

We attribute the branch of the large flux to the L-mode and the branch of the reduced flux to the H-mode. As the gradient increases, the transition from the L-mode to the H-mode occurs as A → B′ → C → C′ → D.

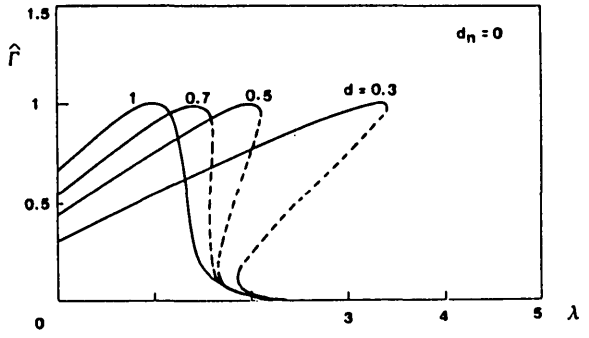

FIG. 4. Normalized particle flux as a function of the edge gradient λ for various values of d (0.3, 0.5, 0.7 and 1). There are no neutral particles, $d_n = 0$.

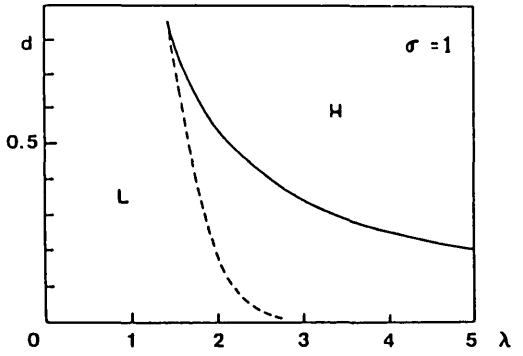

FIG. 5. Boundaries of the L-branch and the H-branch on the d-λ plane ($\sigma = 1$, $d_n = 0$). The solid line is for the L- to H-mode transition and the dashed line is for the H- to L-mode transition.

The H- to L-mode transition occurs as D → C′ → B → B′ → A. There is a hysteresis in the relation of Γ and λ, as shown in Fig. 3, because λ_c for the L- to H-mode transition is larger than λ_c for the H- to L-mode transition. A pedestal develops until the total flux reaches the value q_s. In the limit of Eq. (21), the normalized flux Γ is decreasing function of λ in the H-branch. If the temperature increases, the loss further reduces. On the contrary, if the density increases after the transition, the loss increases with increasing gradient.

Figure 4 illustrates the λ dependence of Γ for various values of d. The critical value λ_c becomes small when d increases. Figure 5 shows the critical value λ_c on the d-λ plane. An approximate condition for the transition is given as

$$\lambda \cdot d \simeq 1 \tag{23}$$

for the L- to H-mode transition ($\sigma = 1$).

The conductive term is also affected by the bifurcation. As shown in Eq. (17), the anomalous electron loss is reduced by the positive radial electric field for a fixed value of the fluctuation level. The mechanism reducing the non-ambipolar part also works for the ambipolar part. On the contrary, the effect of mobility on the ion loss is opposite to that on the electrons. The conductive ion loss increases after the transition.

3.3. Role of neutral particles

Neutral particles cause a loss of toroidally rotating ions. The ion loss increases when the radial electric field is positive. The value of λ necessary for bifurcation becomes large when neutral particle loss is taken into account. This value can be derived from Eq. (18). According to Eq. (17), the solution for positive E_r gives a smaller flux than the solution for negative E_r for given values of d and λ. For the solution of the reduced flux we have the condition

$$\lambda \cdot d \gtrsim 1 + d_n \lambda_i \tag{24}$$

This relation indicates that the critical value λ_c is increased by the contribution of neutral particles.

Figure 6 shows Γ versus λ for various values of d_n. It is noted that the critical value λ_c increases for higher values of d_n and the reduction of Γ across the transition decreases. It is found that a bistable solution exists if d_n is below the value d_n^*:

$$d_n^* = \sqrt{\frac{2\sigma}{e}} - d \tag{25}$$

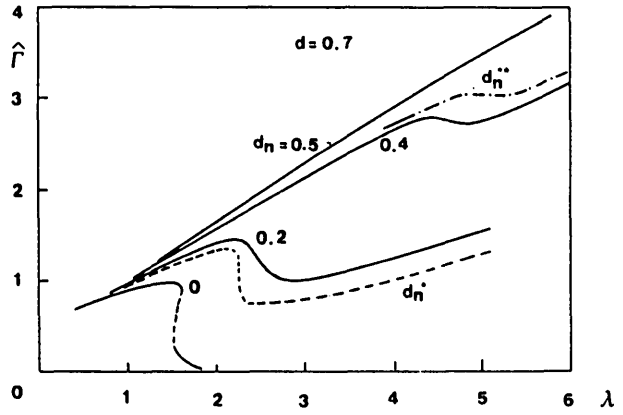

FIG. 6. Normalized flux as a function of the gradient λ in the presence of neutral particles. d_n is chosen as 0, 0.158 (≡ d_n^*), 0.2, 0.4, 0.429 (≡ d_n^{**}), and 0.5, respectively. For $d_n > d_n^{**}$, transition is not possible. σ = 1 and d = 0.7.

If d_n becomes large and the condition

$$d_n < \sqrt{\frac{\sigma}{2e}} \tag{26}$$

i.e.

$$n_0 < \frac{\nu_i F}{\sqrt{\epsilon}\,\langle\sigma_{cx}v\rangle}\,\frac{\rho_p}{\Delta_n}\sqrt{\frac{\sigma}{2e}} \tag{27}$$

is violated, $\hat{\Gamma}$ becomes an increasing function of the gradient λ and no drastic change is expected. In the region $d_n^* < d_n < \sqrt{\sigma/2e}$, a negative slope of $\hat{\Gamma}$, i.e. $\partial\hat{\Gamma}/\partial\lambda < 0$, appears for particular values of λ. The strong transition associated with the bistable states disappears. Equation (27) imposes an upper limit on the neutral density to realize the L- to H-mode transition. The results for the effects of $\Gamma_{i,cx}$ are qualitatively in agreement with those presented in Refs [19, 23].

3.4. Effects of impurities

The transition condition is affected by impurities [46]. One of the mechanisms is the enhancement of the average ionic charge Z_{eff}. When Z_{eff} increases, pitch angle scattering of the bulk ions becomes more frequent and the threshold value λ_c increases. The other mechanism is non-ambipolar loss of impurities. As is pointed out in Ref. [47], the toroidal rotation ejects impurities from the plasma because the toroidal rotation velocity of the impurity ions, which is close to the bulk ion rotation velocity due to ion–ion collisions, can be supersonic for heavy impurities. These effects are studied in Ref. [46], and the approximate condition for the transition in the absence of neutrals is

$$\lambda\cdot d > Z_{eff} + \frac{n_I m_I Z_I}{n_i m_i Z_i} \tag{28}$$

where the suffix I denotes the impurity ion. Including the contribution of neutral particles, Eq. (24) is rewritten as

$$\lambda\cdot d > Z_{eff} + \frac{n_I m_I Z_I}{n_i m_i Z_i} + d_n\lambda_i \tag{29}$$

The value necessary for the gradient to realize the L- to H-mode transition becomes large in the presence of impurities.

4. THRESHOLD POWER

The critical condition for the H-mode transition is given by Eq. (29) (or by Eq. (23) in the case without neutral particles and impurities). The condition is expressed in terms of the local plasma parameters. The confinement law of the L-mode is required for the interpretation of the contribution of the local plasma parameters to the global quantities such as the average plasma density, and to the external parameters such as the heating power. Introducing the relation with the edge parameter and the heating power, we discuss the threshold power for the transition [48].

For simplicity, we assume in the following part that $T_e = T_i$ holds, that the density gradient is evaluated by the penetration length of the neutral particles as $-\nabla n_e/n_e \simeq 1/\Delta_n$, that the temperature gradient is neglected, and that the parameters λ and λ_i are given as $\lambda = \lambda_i = \rho_p/\Delta_n$. Using these approximations, the condition in the case without impurities (Eq. (24)) is rewritten as

$$\frac{\sqrt{\epsilon}\,D_e}{\nu_i\rho_p\Delta_n}\left(1 - \frac{n_0\,\langle\sigma_{cx}v\rangle\,\rho_p\Delta_n}{\sqrt{\epsilon}\,D_e}\right) \gtrsim 1 \tag{30}$$

where the approximation F ≃ 1 is used. Equation (30) implies that the critical condition is a function of the diffusivity at the edge (i.e. the particle confinement time) and of the edge temperature. The critical condition for transition is illustrated in Fig. 5. From the evaluation of λ and from this figure we see that the condition $\rho_p/\Delta_n > 1$, obtained in Ref. [16], is the condition necessary for transition.

4.1. Critical temperature and density

The explicit form of the threshold temperature is derived by introducing the temperature dependences of $\langle\sigma_{cx}v\rangle$, $\langle\sigma_{ion}v\rangle$ and D_e. The temperature dependences of the cross-sections are weak and can be approximated as (see Refs [49, 50])

$$\langle\sigma_{ion}v\rangle \simeq 5 \times 10^{-14}\, T_{100}^{\beta} \tag{31}$$

$$\langle\sigma_{cx}v\rangle \simeq 10^{-14}\, T_{100}^{1/3} \tag{32}$$

In this presentation, T_{100} is the temperature measured in units of 100 eV, and the other parameters are in MKSA units. The exponent β is positive for $T < 100$ eV and $\beta \simeq -1/4$ for $T > 100$ eV. The parameter dependence of D_e is assumed to be $D_e = D_0\sqrt{\epsilon M}\, T^{1.5}/B^2Z$, on the basis of drift wave models [51]. The dependence of D_e on the size and on the safety factor are neglected. Substituting these expressions into Eq. (30), we obtain the equation for the threshold temperature at the edge:

$$T_{100}^{5/2+\beta}\left\{1 - 4.2\left(\frac{RB^2}{a\sqrt{M}\,B_p T_{100}^{2/3+\beta}}\right)\frac{n_0}{n_e}\right\} > \frac{Z^3RB^2}{14MaB_p} \tag{33}$$

where we assume $F \simeq 1$, $D_e = 5\ m^2\cdot s^{-1}$ at $B = 1$ T, and $T = 100$ eV. For present day tokamaks, $T > 100$ eV is needed to satisfy the inequality (33), and we take $\beta = -1/4$. When neutrals are neglected, the threshold temperature can be expressed as

$$T_c\ (\text{eV}) \simeq 100\left(\frac{Z^3RB^2}{14MaB_p}\right)^{4/9} \tag{34}$$

A lower density limit is imposed by neutrals. From Eq. (33), the necessary condition for n_e is derived as

$$\bar{n}_{e19} > 4.2 \times 10^{-3}\frac{qB}{\epsilon^2\sqrt{M}}\, T_{100}^{-5/12}\, n_{016} \tag{35}$$

The other constraint for the existence of a bifurcation is given by Eq. (27). Substituting the temperature dependences into Eq. (27), we obtain

$$\bar{n}_{e19} > \left(\frac{\sigma}{M}\right)^{1/4}\frac{\sqrt{B_p}}{Z}\, T_{100}^{19/24}\sqrt{n_{016}} \tag{36}$$

In Eqs (35) and (36), n_e and n_0 are given in 10^{19} m^{-3} and 10^{16} m^{-3}, respectively. By reducing the neutrals in the main plasma chamber, the lower density limit is decreased.

4.2. Scaling law for the edge parameters

The scaling law for the edge temperature is obtained from an analysis of the SOL plasma. The transition from the edge temperature to the SOL temperature must be continuous at the midplane of the torus. Two-dimensional analyses have been performed analytically and numerically [52, 53]. Assuming that the perpendicular diffusivity has a Bohm-like dependence[1] and that the parallel diffusion is given by the classical value of the collisional plasma in the SOL, the edge temperature scaling is obtained as

$$T \propto \left(\frac{ZB^2P_T^2}{aI_pn_b}\right)^{2/11} \tag{37}$$

where n_b is the density at $r = a$. The power flux P_T is defined as $P_T = P_{heat} - P_{rad} - P_{cx}$, where P_{heat} is the total heating power, and P_{rad} and P_{cx} are the radiation and charge exchange powers from the core plasma. As discussed in Refs [52, 53], the edge temperature increases when the connection length becomes longer, and geometrical parameters such as the aspect ratio also have an influence on the edge temperature. Here, we include only the dependence on the size a and disregard the dependences on R/a or cos θ_m, or on the distance between the limiter/x-point and the wall, etc.

We now discuss the plausibility of the model for D_e. The particle confinement time is given as $\tau_p = a\Delta_n/D_e$. Using Eq. (37), the parameter dependence is predicted as

$$\tau_p \propto a\, B^{1.6}\, n_b^{0.2}\, P_T^{-0.46}\, \bar{n}_e^{-1}\, I_p^{0.2} \tag{38}$$

The particle confinement time in L-mode discharges has been studied in experiments on JT-60 [55, 56]. The dependence of τ_p on P_T, n_e and I_p have been reported as

$$\tau_p \simeq 0.05P_{MW}^{-1/2}\, \bar{n}_{e20}^{-1}\, I_p^0 \tag{39}$$

This shows the power degradation with a similar exponent as in Eq. (38), a weak dependence on I_p

[1] Experimental observations on JET have shown that the cross-field diffusion in the SOL plasma has an approximately Bohm-like dependence [54]. Therefore, we take the Bohm-like model for a first trial.

and a $1/n_e$ dependence. These features support the choice of the parameter dependence of D_e.

4.3. Threshold power for transition

Using the dependence of T on the heating power P_T (Eq. (37)), the critical condition, Eq. (34), for the transition without neutrals is rewritten as

$$P > P_c \tag{40}$$

and P_c scales as

$$P_c \propto \frac{Z^{3.2}B^{1.4}R^{1.2}a^{0.5}n_b^{0.5}}{M^{1.2}I_p^{0.7}} \tag{41}$$

This scaling law suggests that the threshold power becomes high when a or B or Z is increased and that it becomes low when the current or the mass is increased. These observations are not inconsistent with observations in the JFT-2M tokamak [28]. Equation (41) still contains the density at the edge, n_b, which depends more or less on the power and the average density. The scaling given by Eq. (41) is not complete. The edge density depends strongly on the wall conditioning and on the configuration of the plasma chamber. Furthermore, the connection length and the value of σ influence T and n_0 at the edge. These facts may lead to differences in the dependence of P_c from machine to machine. Comparing conditions (37) and (41), it can be seen that a lower critical temperature does not necessarily lead to a lower threshold power. Note that the threshold power P_T is not an additional heating power but the power flowing out of the plasma surface.

5. TEMPORAL EVOLUTION

The ambipolarity equation shows that multiple solutions exist in the stationary state. In connection with the bifurcation of the solution, we have three typical time-scales. One of them is the time-scale of the change of the electric field at $\lambda = \lambda_c$. The ion distribution function is newly formed in connection with the development of E_r. These changes are rapid processes, and the other background plasma parameters are assumed to be constant during the change of the electric field. For the evolution of the plasma parameters after the change of the solution from the L-branch to the H-branch we have another time-scale. This is related to the formation of a pedestal at the edge. The time-scales may change, depending on the typical lengths of the structures of interest. In this section, we consider one example of the temporal evolution in the absence of neutrals.

5.1. Change of the electric field

Integrating the Poisson equation and the continuity equation of the charge, we obtain the equation for predicting the temporal evolution of the radial electric field. A strong electric field is predicted in the H-branch by Eq. (22). The process considered in Section 3 is expected to occur in the narrow region near the surface, Δ, and the electric field may also be localized near the edge. The ion viscosity becomes important if the localization is too strong. For the evolution of the radial electric field we take the radial diffusion of the $E \times B$ rotation into account. Writing the viscosity damping term as $\mu_\perp \nabla^2(R\omega_E)$, we have

$$\frac{\epsilon_0\epsilon_\perp}{e}\frac{\partial E_r}{\partial t} = \left[\frac{\nu_i\rho_p n_i}{\sqrt{\epsilon}}(\hat{\Gamma}_e - \hat{\Gamma}_i) + \frac{\rho_p n_i}{v_{Ti}}\mu_\perp \nabla^2(R\omega_E)\right] \tag{42}$$

where $\epsilon_\perp$ is the dielectric constant of the magnetized plasma. The ion polarization drift is taken into account and $\epsilon_\perp$ is given as $1 + c^2/v_A^2$, where v_A is the Alfvén velocity and c is the velocity of light. In the neoclassical limit, $\mu_\perp$ is evaluated as $\nu_i\rho_i^2q^2/10$ [40]. Instead of solving the partial differential equation, we evaluate the time-scale by introducing the typical thickness of the layer. This layer thickness is characterized by the region where direct loss of ions occurs. The operator $\partial^2/\partial r^2$ is replaced by the value $1/\Delta^2$. Choosing Δ as ρ_p, the viscosity damping term in the absence of neutrals is estimated as $-(\nu_i\epsilon^2/10)(R\omega_E/v_{Ti})\rho_p n_i$ in Γ_i.

If λ becomes slightly larger than λ_c, the first term on the right hand side of Eq. (42) becomes large and an electric field is generated. Introducing normalized parameters, we obtain the equation showing the transition from C to C′:

$$\frac{\partial}{\partial\tau}X = \hat{\Gamma}_e(X) - \hat{\Gamma}_i(X) - \frac{\mu_\perp}{\nu_i\rho_p^2}X \tag{43}$$

where

$$\tau = t/\tau_{tr} \tag{44a}$$

$$\tau_{tr} = \frac{T_i\epsilon_\perp\epsilon_0\sqrt{\epsilon}}{e^2\rho_p^2 n_i\nu_i F} \sim \frac{\epsilon^{5/2}}{Fq^2\nu_i} \tag{44b}$$

For $\lambda = \lambda_c + 0$, the driving term of the electric field (first and second terms of Eq. (43)), is much larger than the viscosity damping term, as long as neoclassical viscosity is assumed. The typical time-scale τ_{tr} for the parameters of ASDEX, R = 1.6 m, a = 0.4, B = 2.5 T, q = 3, T = 0.5 keV and $n_e = 3 \times 10^{19}$ m^{-3}, is about 30 μs. The time constant is close to this value even in larger devices such as JET or DIII-D. The redistribution time of ions in velocity space is of a similar order as τ_{tr}.

From this relation, we see that the transition from the L-branch to the H-branch occurs much faster than viscosity damping could account for. Our neglect of viscosity damping in Eq. (18) and the 0-D modelling are justified by this result. When neutrals are present, τ_{tr} becomes longer because the associated jump of the flux $\hat{\Gamma}$ becomes smaller (see Fig. 6).

5.2. Development of a pedestal

As is shown in Figs 3 and 6, the particle flux out of the plasma is greatly reduced after the transition from C to C′. The reduction of the flux occurs in a short period, as is predicted by Eq. (43). During this period, the background plasma parameters are unchanged, except for the toroidal rotation. After the transition C → C′ and the establishment of the electric field, the particle flux and the convective energy loss become small. The flux out of the plasma, q_{out}, becomes smaller than the supply of particles from the core plasma, q_s, defined by

$$q_s = \frac{1}{4\pi^2 aR}(P_{heat} - P_{rad} - P_{cx}) \tag{45}$$

The sudden increase in $q_s - q_{out}$ causes an increase in the edge temperature and a growth of the density pedestal. The pedestal develops until the total flux reaches the value q_s. The pedestal formation of the density and temperature depends on the condition of n_0 and the anomalous transport processes near the edge.

5.3. Impurity accumulation, edge localized mode and H- to L-mode transition

If the H-mode continues for a long time, the impurity level increases. The period of edge localized modes (ELMs) depends on the form of the impurity accumulation [57, 58]. The electric bifurcation model has been used to explain the impurity accumulation and the ELMs [46].

The steep gradient near the edge can cause an inward drift of impurities. For instance, neoclassical theory [59] predicts that the inward drift continues until the impurity gradient reaches a value given by

$$\frac{1}{p_I}\frac{dp_I}{dr} = \frac{Z_I}{p_i}\frac{dp_i}{dr} \tag{46}$$

This impurity accumulation affects the transition condition [48]. We consider here the transition from the H-branch to the L-branch. As Eq. (46) shows, impurities have a long confinement time in the H-phase. The supply of impurities from the SOL plasma can cause an increase in Z_{eff}. The impurity diffusion can be anomalous and the rate of change of Z_{eff} can be different from the neoclassical prediction [60]. We therefore take dZ_{eff}/dt as a parameter and estimate the time τ_Z for the transition to the L-branch. We consider the case of light impurities in hydrogen plasmas, for which $m_I/m_i \simeq 2Z_I$. Assume that the edge parameter reaches point D in Fig. 7 ($\lambda = \lambda_D$) after the onset of the H-mode transition with $Z_{eff} = 1$. The critical condition for λ changes according to Eq. (29) and is rewritten as $(3Z_{eff} - 2) + d_n\lambda_i = d\lambda_D$ for the H- to L-mode transition. Correcting this equation for the case of pure hydrogen (Eq. (24) with $\lambda = \lambda_c$), the threshold value of Z_{eff} for the L-mode transition is estimated as

$$Z_{eff} \simeq \frac{d}{3}(\lambda_D - \lambda_c) + 1 \tag{47}$$

where $\lambda_i \simeq \lambda$ is assumed for simplicity. Using the accumulation rate dZ_{eff}/dt, τ_Z is estimated as

$$\tau_Z = \frac{1}{|dZ_{eff}/dt|}\frac{d}{3}(\lambda_D - \lambda_c) \tag{48}$$

which gives the approximate duration of the H-phase.

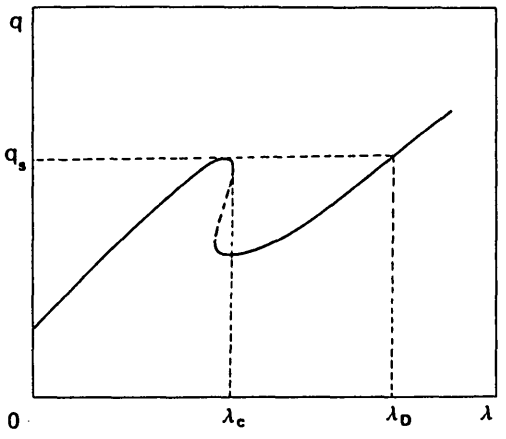

FIG. 7. Illustration of the balance point λ_D.

This increase of impurities is the process occurring near the plasma surface.

After the H- to L-transition, the pedestal plasma disappears within a time-scale of $\tau_{burst} = \Delta^2/D_e$. The impurities are also lost from the edge plasma. Comparing the speed of the reduction in bulk plasma and impurities, we see that Eq. (24) is satisfied again with a time-scale of τ_{burst} if the condition for these reduction rates

$$\frac{dZ_{eff}}{dt} < \frac{1}{3}\frac{d}{dt}(\lambda \cdot d) \tag{49}$$

is satisfied. This rapid disappearance/formation of the pedestal plasma can be regarded as a kind of ELM.

In the core plasma, the radiation loss gradually increases, mainly because of the density increase or the pile-up of impurities. If the radiation from the core plasma becomes high and q_s becomes smaller than the critical flux q_c, transition from the L-mode to the H-mode is impossible. Measurements in JFT-2M have shown that the H-mode terminates during additional heating if the total radiation power loss approaches the heating power [61].

6. SUMMARY AND DISCUSSION

In this paper we have studied a theoretical model of the H-mode in tokamaks, based on the bifurcation of the radial electric field at the edge. The edge region is characterized by non-ambipolar fluxes of ions and electrons, which determine the radial electric field. We have studied the effect of the radial electric field on the ion loss in the loss cone. If a correction of the order of ϵ is taken into account, the loss can be reduced by the toroidal motion of ions. It is found that bifurcations of the radial electric field, the particle flux and the convective energy flux at the edge can occur if the edge gradient reaches a critical value.

The critical temperature and the density threshold for the L- to H-mode transition have been obtained. The neutral density imposes a lower density limit. The critical temperature is incorporated in the necessary power. Using combined analyses of the SOL plasma and the particle confinement time, the critical condition is expressed in terms of the power flowing out of the plasma edge, i.e the threshold power is derived. The threshold power is an increasing function of a, B, Z, $1/I_p$ and 1/M. The analysis also indicates the importance of reducing the neutral density for realizing H-mode operation. In the estimate of P_c the effect of ∇T is neglected. For a precise comparison with experiments, further calculations are necessary.

The temporal evolution has also been studied. When the parameter λ reaches a critical value, λ_c, rapid transition occurs. The typical time-scale for present-day tokamaks to move from the L-branch to the H-branch is estimated to be 30 μs. The ions are redistributed in velocity space with a similar time constant. These time constants are the shortest of the various time-scales associated with the H-mode. After the change of the radial electric field and the fluxes, the parameters of the background plasma (except for the toroidal rotation) change with the time-scale of the transport across the thin layer near the edge. The formation of a pedestal at the edge causes an accumulation of impurities, which may trigger the onset of the H- to L-mode transition.

Theoretical estimates of the threshold power have been presented in previous articles. Taking into account the edge ion loss, $P_c \propto n^2a^2R/I_p$ is obtained in Ref. [19]. Starting from the relation $\nu^* = 1$ and evaluating ν^* from the volume averaged temperature, $P_c \propto n^3qa^{3.3}R/I_p^2M$ is derived [23]. We have used here a scaling of the edge parameter to obtain Eq. (41). References [19] and [23] are in qualitative agreement with our results, i.e. P_s is an increasing function of n, B_t, a, R, $1/I_p$ and 1/M. The dependences are, however, much stronger than in our case. Recently, Shimizu et al. [62] simulated the evolution of an NBI heated plasma in JT-60 with a transport code. They combined the critical conditions derived by our model with the simulation and compared the predicted occurrence of the H-mode with experimental results. Good agreement is found for the threshold power and the delay time of the transition after the onset of NBI.

We have chosen D_e as an increasing function of T to study the particle confinement time of the L-mode, which also shows a power degradation (Eq. (39)). When the temperature is much lower, of the order of 10 eV, resistively driven (such as resistivity gradient driven) turbulence may be important and D_e has a different dependence on T [60, 63]. The critical temperature for transition obtained here (Eq. (34)) is much higher (typically a few hundred electronvolts). In this regime, the rippling mode is stabilized [64] and resistive modes are less important because of the higher temperature. The dependence $D_e \propto T^{1.5}$ is used for the L-mode and is in agreement with τ_p of JT-60. A more accurate form of D_e will give a better estimate of the transition condition.

In our model it is assumed that the edge fluctuations are not the primary cause of the transition. In experiments, a sudden change in the edge fluctuations has been observed which may cause a change in the edge transport. For the H-phase, another kind of diffusivity may apply. A possible mechanism for reducing the fluctuations associated with trapped particle instability is discussed in Ref. [65], but more thorough work is needed.

Our conclusions depend on the specific non-linearity of Eq. (18). The electric field effect is taken into account to satisfy Einstein's relation. The E_r dependence of D_e, for instance, is neglected. If effects of fluctuations, such as D_e (E_r), are introduced, the threshold condition would be quantitatively affected. For instance, a temporal change in D_e would affect the time development of the H-mode. If the value of D_e during the H-phase is reduced, with the other parameters fixed, the H-phase may jump back to the L-phase and vice versa. This suggests an oscillatory behaviour of H/L transitions. The relation between grassy ELMs and this conjecture has to be studied.

The inhomogeneity of the radial electric field can also have a strong effect on the ion loss. The banana width is reduced when u_g is negative [22]. The radial structure of the electric field has not been taken into account in our investigations. We have introduced typical scale lengths which govern the H-mode, for example Δ, Δ_n, ρ_p, ρ_b. The parameter dependence of the time-scale of τ_{tr}, τ_E, τ_p, etc. would be affected by a different choice of scale lengths. An extension of the bifurcation model to include the radial structure and the effect on the fluctuations is planned.

Appendix

ION ORBIT NEAR THE BOUNDARY

The ion orbit near the boundary in the presence of a radial electric field is studied. The magnetic flux ψ is introduced as $yB_p = -d\psi/dy$ ($y = R + r\cos\theta$). In a frame which is rotating in the toroidal direction with frequency ω_E, there are the following constants of motion [22]:

$$W = \frac{m}{2}(v_\parallel^2 + v_\perp^2) - \frac{e}{2}\frac{dE_r}{dr}\left(\frac{\psi - \psi_0}{\partial\psi/\partial r}\right)^2 - \frac{m}{2}\omega_E^2 y^2 \qquad \text{(A-1)}$$

$$\psi_* = \psi - \frac{m}{e}\left[\frac{yB_\phi}{B}v_\parallel + \omega_E y^2\right] \qquad \text{(A-2)}$$

and the adiabatic invariance is

$$\mu = \frac{v_\perp^2}{2B} \qquad \text{(A-3)}$$

The deviation of the orbit from the magnetic surface is calculated by using the invariances W, ψ_* and μ.

The quantities at the outside of the torus, $\theta = 0$, are denoted by the suffix zero. We write $r = r_0 + \delta$, and expand Eqs (A-1) to (A-3) with respect to ϵ and δ. Eliminating $v_\perp$, we have the normalized forms of δ and $v_\parallel$ as

$$u_\parallel^2 = u_{\parallel 0}^2 - \epsilon(1 - \cos\theta)(u_{\perp 0}^2 + 2u_E^2) + u_g\delta^2 \qquad \text{(A-4)}$$

$$\delta = (u_{\parallel 0} - u_\parallel)(1 - \epsilon\Lambda\cos\theta) + 2\epsilon(1 - \cos\theta)u_E \qquad \text{(A-5)}$$

where $\vec{u} = \vec{v}/v_{Ti}$, $u_E = \omega_E R/v_{Ti}$ and $u_g = \rho_p(dE_r/dr)/v_{Ti}B_p$. The correction u_E is the effect of the centrifugal force by $E \times B$ rotation, and u_g is the contribution of the electric field gradient. The guiding centre drift equation is valid in the limit $u_g \ll 1$.

This equation shows that the counter-travelling particles ($u_\parallel > 0$) deviate from the original magnetic surface outwards. Because of the existence of a centrifugal force, the region of trapped particles in velocity space becomes wider. The boundary between trapped and transit particles in the case of $u_g = 0$ is given (up to the accuracy of $\sqrt{\epsilon}$) by

$$u_{\parallel 0}^2 = \epsilon(1 - \cos\theta)(u_{\perp 0}^2 + 2u_E^2) \qquad \text{(A-6)}$$

and becomes hyperbolic. It is noted that if the turning point of the banana orbit, θ_b, is smaller than θ_m, the particles do not interact with the limiter (or are not diverted to the divertor plate) and are not lost. If this is the case, the distance between the plasma surface and the chamber is, of course, longer than ρ_p and therefore the loss cone is localized in velocity space. The conditions for particles to be lost are

$$\epsilon(1 - \cos\theta_m) < \frac{u_{\parallel 0}^2}{u_{\perp 0}^2 + 2u_E^2} < 2\epsilon \qquad \text{(A-7)}$$

and particles satisfying the condition $u_{l0} < u_c$ are lost,

$$u_c = \sqrt{2\epsilon(1 - \cos\theta_m)}\, u_E \qquad \text{(A-8)}$$

The value of u_c is the minimum velocity of the loss cone in the rotating frame. Figure A-1 illustrates the regime of the loss cone in the rotating frame.

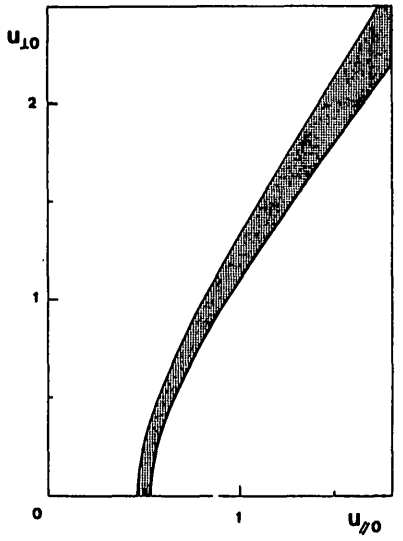

FIG. A-1. Region of the loss cone in velocity space in the rotating frame.

The gradient of the electric field also affects the loss region [22]. Substituting the condition $u_{//} = 0$ at $\theta = \theta_m$ into Eq. (A-8), this is rewritten as

$$\frac{u_{l0}^2}{u_{\perp 0}^2 + 2u_E^2} = \frac{\epsilon(1 - \cos\theta_m)}{1 + u_g} \quad (u_g \ll 1) \qquad \text{(A-9)}$$

If the sign of u_g is positive, the edge of the loss cone is closer to the origin.

The bounce frequency of trapped particles increases when a radial electric field is present. The bounce frequency of deeply trapped particles is given from Eqs (A-4) and (A-5) as

$$\omega_b = \sqrt{\frac{\epsilon}{2}}\,\frac{v_{Ti}}{qR}\,\sqrt{u_{\perp 0}^2 + 2u_E^2} \qquad \text{(A-10)}$$

The averaged bounce frequency as given by the relation $\langle u_{\perp 0}^2 \rangle = 1$ is

$$\bar{\omega}_b = \sqrt{\frac{\epsilon}{2}}\,\frac{v_{Ti}}{qR}\,\sqrt{1 + 2u_E^2} \qquad \text{(A-11)}$$

The normalized collisionality, $\nu_* = \nu_i/\bar{\omega}_b$, becomes $1/\sqrt{1 + 2u_E^2}$ times smaller and the collisionless regime becomes wider because of the influence of the electric field.

ACKNOWLEDGEMENTS

The authors wish to thank Dr. F. Wagner for his help in realizing this project and for stimulating discussions. Thanks are also due to Dr. K. Lackner, Dr. T. Ohkawa and Dr. F.L. Hinton for elucidating and creative discussions. Also acknowledged are discussions with members of the ASDEX group, Drs M. Shimada, S. Tsuji, M. Azumi, Y. Miura, K. Toi, N. Suzuki, D. Düchs and M. Wakatani. The authors are also grateful to the referees for their comments, to Dr. S. Yoshikawa for continuous guidance, and to Dr. A. Iiyoshi and Dr. K. Nishikawa for encouragement.

This work has been partly supported by a Grant-in-Aid for Fusion Research and a Grant-in-Aid for Scientific Research of the Ministry of Education, Science and Culture of Japan.

REFERENCES

[1] WAGNER, F., BECKER, G., BEHRINGER, K., et al., Phys. Rev. Lett. **49** (1982) 1408.

[2] BURRELL, K.H., in Controlled Fusion and Plasma Physics (Proc. 11th Eur. Conf. Aachen, 1983), Vol. 7, Part I, European Physical Society (1983) 11.

[3] KAYE, S.M., BELL, M., BOL, K., et al., ibid., p. 19.

[4] McGUIRE, K., BEIERSDORFER, P., BELL, M., et al., in Plasma Physics and Controlled Nuclear Fusion Research 1984 (Proc. 10th Int. Conf. London, 1984), Vol. 1, IAEA, Vienna (1985) 117.

[5] MIURA, Y., and JFT-2M Group, Characteristics of Improved Confinement and High Beta in Pellet and Neutral-Beam Injected Single Null Divertor Discharges of JFT-2M Tokamak, Res. Rep. JAERI-M 86-148, Japan Atomic Energy Research Institute (1986).

[6] LUXON, J., ANDERSON, P., BATTY, F., et al., in Plasma Physics and Controlled Nuclear Fusion Research 1986 (Proc. 11th Int. Conf. Kyoto, 1986), Vol. 1, IAEA, Vienna (1987) 159.

[7] TANGA, A., BARTLETT, D.V., BEHRINGER, K., et al., ibid., p 65.

[8] JT-60 Team, Plasma Phys. Controll. Fusion **30** (1988) 1405.

[9] WAGNER, F., and ASDEX- and NBI-Teams, in Basic Physical Processes of Toroidal Fusion Plasmas (Proc. Workshop Varenna, 1985), Vol. 1, CEC, Luxembourg (1986) 61.
[10] OKAMOTO, M., AZUMI, M., NAGAMI, M., SUZUKI, N., MATSUMOTO, H., Kakuyugo Kenkyu **58** (1987) 105 (in Japanese).
[11] KEILHACKER, M., BECKER, G., BERNHARDI, K., et al., Plasma Phys. Controll. Fusion **26** (1984) 49.
[12] ITOH, S.-I., TSUJI, S., ITOH, K., Kakuyugo Kenkyu **59** (1988) 244 (in Japanese).
[13] OHKAWA, T., HINTON, F.L., LIU, C.S., LEE, Y.C., Phys. Rev. Lett. **51** (1983) 2101.
[14] HINTON, F.L., CHU, M.S., DOMINGUEZ, R.R., et al., in Plasma Physics and Controlled Nuclear Fusion Research 1984 (Proc. 10th Int. Conf. London, 1984), Vol. 2, IAEA, Vienna (1985) 3.
[15] HINTON, F.L., Nucl. Fusion **25** (1985) 1457.
[16] OHKAWA, T., Kakuyugo Kenkyu **56** (1986) 274.
[17] OHKAWA, T., Kakuyugo Kenkyu **56** (1986) 427.
[18] BISHOP, C.M., Nucl. Fusion **26** (1986) 1063.
[19] OHKAWA, T., HINTON, F.L., in Plasma Physics and Controlled Nuclear Fusion Research 1986 (Proc. 11th Int. Conf. Kyoto, 1986), Vol. 2, IAEA, Vienna (1987) 221.
[20] HAHM, T.S., DIAMOND, P.H., Phys. Fluids **30** (1987) 133.
[21] ITOH, S.-I., ITOH, K., Phys. Rev. Lett. **60** (1988) 2276.
[22] HINTON, F.L., "Ion-electron energy transfer near the separatrix in diverted tokamaks", paper presented at Sherwood Theory Meeting, Oak Ridge, TN, 1987.
[23] SHAING, K.C., HOULBERG, W.A., CRUME, E.C., Comments Plasma Phys. Controll. Fusion **12** (1988) 69.
[24] WAGNER, F., FUSSMANN, G., GRAVE, T., et al., Phys. Rev. Lett. **53** (1984) 1453.
[25] KEILHACKER, M., GIERKE, G. von, MÜLLER, E.R., et al., Plasma Phys. Controll. Fusion **28** (1986) 29.
[26] BURRELL, K.H., PRATER, R., GOHIL, P., OHYABU, N., BROOKS, N.H., "H-mode overview of DIII-D presentations to H-mode Workshop", paper presented at H-mode Workshop, San Diego, CA, 1987.
[27] ODAJIMA, K., FUNAHASHI, A., HOSHINO, K., et al., in Plasma Physics and Controlled Nuclear Fusion Research 1986 (Proc. 11th Int. Conf. Kyoto, 1986), Vol. 1, IAEA, Vienna (1987) 151.
[28] SUZUKI, N., and JFT-2M Group, in Controlled Fusion and Plasma Physics (Proc. 14th Eur. Conf. Madrid, 1987), Vol. 11D, Part I, European Physical Society (1987) 217.
[29] LACKNER, K., DITTE, U., FUSSMANN, G., et al., in Plasma Physics and Controlled Nuclear Fusion Research 1984 (Proc. 10th Int. Conf. London, 1984), Vol. 1, IAEA, Vienna (1985) 319.
[30] TANGA, A., BEHRINGER, K.H., COSTLEY, A.E., et al., Nucl. Fusion **27** (1987) 1877.
[31] WAGNER, F., BARTIROMO, R., BECKER, G., et al., Nucl. Fusion **25** (1985) 1490.
[32] HOSHINO, K., YAMAMOTO, T., KAWASHIMA, H., et al., J. Phys. Soc. Jpn **56** (1987) 1750.
[33] BHATNAGAR, V.P., ODAJIMA, K., ELLIS, J.J., JACQUINOT, J., START, D.F.H., Bull. Am. Phys. Soc. **32** (1987) 5V5.
[34] TOI, K., GERNHARDT, J., KLÜBER, O., KORNHERR, M., "Precursor oscillation to H-mode transition in ASDEX", paper presented at Annual Meeting of the Physical Society of Japan, Koriyama, 1988 (in Japanese).
[35] HAZELTINE, R.D., HINTON, F.L., Phys. Fluids **16** (1973) 1883.
[36] TUDA, T., Theory on Radial Electric Field and Impurity Transport in Tokamaks, Res. Rep. JAERI-M 8750, Japan Atomic Energy Research Institute (1980) (in Japanese).
[37] HIRSHMAN, S.P., Nucl. Fusion **18** (1978) 917.
[38] HINTON, F.L., WONG, S.K., Phys. Fluids **28** (1985) 3082.
[39] HINTON, F.L., Itoh Theory of L-H Transition, General Atomics Theory Memo, Aug. 1988.
[40] CHIUEH, T., TERRY, P.W., DIAMOND, P.H., SEDLAK, J.E., Phys. Fluids **29** (1986) 231.
[41] INOUE, S., TANGE, T., ITOH, K., TUDA, T., Nucl. Fusion **19** (1979) 1252.
[42] HORTON, C.W., Plasma Phys. **22** (1980) 345.
[43] WALTZ, R.E., Phys. Fluids **25** (1982) 1269.
[44] THOM, R., Structural Stability and Morphogenesis (FOWLER, D.H., Transl.), Benjamin, New York (1975) Sect. 5.
[45] STRINGER, T.E., Phys. Fluids **13** (1970) 1586.
[46] OHKAWA, T., ITOH, K., ITOH, S.-I., Kakuyugo Kenkyu **59** (1988) 487.
[47] YOSHIKAWA, S., Impurity Ions in a Rotating Tokamak, Res. Rep. PPPL-1710, Princeton Plasma Physics Laboratory, Princeton, NJ (1980).
[48] ITOH, K., ITOH, S.-I., Plasma Phys. Controll. Fusion **31** (1989) 487.
[49] HARRISON, M.F.A., in Atomic and Molecular Physics of Controlled Thermonuclear Fusion, Plenum Press, New York (1983).
[50] FREEMAN, R.L., JONES, E.M., Atomic Processes in Plasma Physics Experiments I., Rep. R137, Culham Laboratory, UKAEA, Abingdon, Oxfordshire (1974).
[51] HORTON, C.W., in Handbook of Plasma Physics, Vol. 2, Basic Plasma Physics, North-Holland, Amsterdam (1984) Sect. 6.4.
[52] WAGNER, F., LACKNER, K., in Physics of Plasma Wall Interactions in Controlled Fusion, NATO ASI Series B131, Plenum Press, New York (1984) 931.
[53] UEDA, N., ITOH, K., ITOH, S.-I., Nucl. Fusion **29** (1989) 173.
[54] TAGLE, J.A., ERENTS, K.S., McCRACKEN, G.M., et al., in Controlled Fusion and Plasma Physics (Proc. 14th Eur. Conf. Madrid, 1987), Vol. 11D, Part II, European Physical Society (1987) 662.
[55] TSUJI, S., and JT-60 Team, ibid., Part I, p. 57.
[56] NAKAMURA, H., and JT-60 Team, Nucl. Fusion **28** (1988) 43.
[57] MÜLLER, R.E., KEILHACKER, M., STEINMETZ, K., the ASDEX and NI Teams, J. Nucl. Mater. **121** (1984) 138.
[58] BROOKS, N., BURRELL, K.H., LEE, P., et al., Bull. Am. Phys. Soc. **32** (1987) 1898.
[59] RUTHERFORD, P.H., Phys. Fluids **17** (1974) 1782.
[60] HAHM, T.S., DIAMOND, P.H., TERRY, P.W., GARCIA, L., CARRERAS, B.A., Phys. Fluids **30** (1987) 1452.

[61] TAMAI, M., and JFT-2M Group, "Behaviour of the radiation loss during H-mode phase in the JFT-2M tokamak", paper presented at Annual Meeting of the Japan Society of Plasma Science and Nuclear Fusion Researach, Kyoto, 1987 (in Japanese).
[62] SHIMIZU, K., HIRAYAMA, T., SHIRAI, H., AZUMI, M., and JT-60 Team, "Numerical simulation of L/H transition in divertor discharges", J. Nucl. Mater., in press.
[63] ROGISTER, A., Plasma Phys. Controll. Fusion **28** (1986) 547.
[64] HIROSE, A., KROEKER, T.L., Phys. Fluids **30** (1987) 3752.
[65] ITOH, S.-I., ITOH, K., OHKAWA, T., UEDA, N., in Plasma Physics and Controlled Nuclear Fusion Research 1988 (Proc. 12th Int. Conf. Nice, 1988), Paper IAEA-CN-50/D-I-3, Vol. 2, IAEA, Vienna (to be published).

(Manuscript received 19 September 1988
Final manuscript received 1 March 1989)